NREL
NATIONAL RENEWABLE ENERGY LABORATORY

Solar Ramping Distributions over Multiple Timescales and Weather Patterns

Bri-Mathias Hodge, Marissa Hummon, and Kirsten Orwig
National Renewable Energy Laboratory

Presented at the 10th International Workshop on Large-Scale Integration of Wind Power into Power Systems
Aarhus, Denmark
October 25 – 26, 2011

NREL is a national laboratory of the U.S. Department of Energy
Office of Energy Efficiency & Renewable Energy
Operated by the Alliance for Sustainable Energy, LLC

This report is available at no cost from the National Renewable Energy Laboratory (NREL) at www.nrel.gov/publications.

Conference Paper
NREL/CP-5500-52735
February 2015

Contract No. DE-AC36-08GO28308

NOTICE

This report is available at no cost from the National Renewable Energy Laboratory (NREL) at www.nrel.gov/publications.

Available electronically at http://www.osti.gov/scitech

Available for a processing fee to U.S. Department of Energy and its contractors, in paper, from:

U.S. Department of Energy
Office of Scientific and Technical Information
P.O. Box 62
Oak Ridge, TN 37831-0062
phone: 865.576.8401
fax: 865.576.5728
email: mailto:reports@adonis.osti.gov

Available for sale to the public, in paper, from:

U.S. Department of Commerce
National Technical Information Service
5285 Port Royal Road
Springfield, VA 22161
phone: 800.553.6847
fax: 703.605.6900
email: orders@ntis.fedworld.gov
online ordering: http://www.ntis.gov/help/ordermethods.aspx

Cover Photos: (left to right) photo by Pat Corkery, NREL 16416, photo from SunEdison, NREL 17423, photo by Pat Corkery, NREL 16560, photo by Dennis Schroeder, NREL 17613, photo by Dean Armstrong, NREL 17436, photo by Pat Corkery, NREL 17721.

Solar Ramping Distributions over Multiple Timescales and Weather Patterns

Bri-Mathias Hodge, Marissa Hummon, and Kirsten Orwig

***Abstract* — As greater amounts of solar power are included in the power system, it is becoming increasingly important to have a better characterization of the variability of solar power over the timescales that are relevant to power system operations. In this paper, we examine the distribution of ramp events that occur in global horizontal irradiance measurements from a number of sites in the western United States. The distributions are found to be significantly non-normal over multiple timescales from 1 minute to 1 hour. A hyberbolic distribution is suggested for more accurately representing the observed ramp distributions. Additionally, the ramp distributions that occur during different classifications of weather patterns are characterized and significant differences are observed between patterns.**

***Index Terms*—Solar photovoltaic power generation, stochastic systems**

I. Introduction

Solar photovoltaic (PV) power is expected to play an increasing role in power systems operations over the coming decade. The variable and uncertain nature of PV power output may present issues in maintaining the continued reliable system operation at higher penetration levels of solar PV power. One important consideration in solar PV integration is the characterization of how the plant output can change over multiple timescales and during different weather patterns. A better understanding of the ramps that may occur in PV power output can help in creating better solar power forecasts, as well as help the system operator decide on the reserve levels necessary to counteract any changes in PV output levels. In addition, better characterization of solar ramps can lead to more realistic synthesized datasets in solar integration studies. Mills et al. provides a general overview of the implications of PV integration into the larger power system, as well as a summary of the current state of knowledge in the field [1].

One important consideration in the analysis of solar PV power and irradiance data is the impact of geographic smoothing of PV power output. Since at very short timescales (such as 1 minute) solar irradiance is not perfectly correlated, even between sites that are very close together, the combined output of multiple plants has smaller magnitude ramps in output than individual sites. This geographic smoothing is noticeable even at relatively small scales such as between a single pyranometer and a PV plant. For example, Marcos et al. examined one year's worth of power and irradiance data from six PV plants in Spain at the 1-second timescale [2]. They found that the power output was much smoother than the irradiance measurements due to the smoothing effect of the relatively large plant sizes (from 775 kW to 7.2 MW) compared to the point irradiance measurements. Subsequent work by the same authors modeled the smoothing effect as a low pass filter to create a model that can simulate the power output of a PV plant of different sizes from irradiance data [3]. This geographic smoothing is even more pronounced when the distances involved are on the scale of those between cities. Wiemken et al. examined the 5-minute power fluctuations from 100 small PV plants spread out over Germany [4]. While individual systems could experience 5-minute power output changes of up to 50% of installed capacity, the combined 100 systems did not have any events above 5% of capacity. Curtright and Apt used a power spectral density approach to investigate the ramps in four PV systems situated in Arizona [5]. They concluded that the power fluctuations in the range of 10 minutes to several hours were greater for PV systems than for wind systems, based on the slope of the power spectra observed. Lave and Kleissl examine the individual and aggregate ramp rates of global horizontal irradiance (GHI) at four locations in the state of Colorado [6], including two used in this work. A power spectral analysis was conducted and the aggregated output from the four sites was found to be smoother than the GHI ramps observed at each of the individual sites. While the aforementioned studies have tended to focus on GHI, others have examined the related issues of clearness index distributions [7] and fluctuations in the clearness index [8].

In this paper, we focus only on the changes in irradiance at single sites. The ramps in irradiance are statistically characterized for different short-term timescales, from 1-minute to 1-hour averages. Additionally, the ramps that can be expected during different weather patterns are also characterized, as they can differ widely, for example between clear sky and overcast days. Using statistical measures beyond the mean and standard deviation to help characterize the distributions is an important component of the analysis. Many integration studies make an implicit assumption that a solar related variable is normally distributed by using the standard deviation as the sole metric [9]. As will be demonstrated in Section III, this may be a very poor assumption. Solar data distributions can vary strongly depending on both the timescale and geographic aggregation under consideration. Therefore, it is important to first analyze the observed distributions for the questions under study before choosing a model distribution.

The remainder of the paper is organized as follows. In Section II, the methods and data used in this study are detailed. Section III reports on the results of analyzing the ramping event distributions over different timescales and

The authors are with the National Renewable Energy Laboratory, Golden, CO 8041 USA (email: bri-mathias.hodge@nrel.gov, marissa.hummon@nrel.gov, kirsten.orwig@nrel.gov)

weather patterns, and demonstrates the effectiveness of modeling the observed ramping distributions with a model distribution. Conclusions are then drawn and future areas for examination outlined in Section IV.

II. Methods and Data

In this section, some of the important methods utilized in the study are described. Section II-A contains information on the datasets analyzed. Section II-B gives some statistical background that may be aid the reader in understanding the subsequent results.

A. Data Utilized

In this paper, we have examined solar irradiance data exclusively from the Western Interconnection area in the United States, utilizing data from the National Renewable Energy Laboratory's (NREL) Measurement and Instrumentation Data Center [10]. Each dataset contains 1 year of GHI data at the one minute resolution level. GHI data consists of two different components: the direct normal irradiance and the diffuse horizontal irradiance. While for concentrating solar plants, only the direct normal irradiance is important, both components contribute for solar PV plants, and thus changes in GHI are examined in this study. Seven different sites are included in the datasets, as summarized in Table I. The sites include: Solar Radiation Research Laboratory (SRRL), National Wind Technology Center (NWTC), Nevada Power Clark Station (NPCS), University of Nevada, Las Vegas (UNLV), Humboldt State University (HSU), Loyola Marymount University (LMU), and Sun Spot One (SSO). Most sites have multiple years of data, resulting in 26 total datasets. The datasets studied are all one full year of observed 1-minute GHI readings between the years 2005 to 2010. Corresponding clear sky profiles were created for all of the datasets using the Bird clear sky model [11]. This data represents the expected amount of GHI that would be seen at each site based on the assumption of a clear sky, the location of the site, and the time of day and year. The difference between the expected clear sky values and the observed 1-minute GHI values may be seen in Fig. 1. While this method does not predict exact clear sky spectra, it is suitable for our purposes where no additional atmospheric measurements are available. This clear sky data is used to remove the expected ramps in irradiance due to diurnal patterns out of the data sets. Therefore, all subsequent discussion of irradiance ramps refers only to the unexpected ramps, i.e., those not due to diurnal patterns.

TABLE I
Location and Years for the Datasets Used in the Analysis

Site	Location	'05	'06	'07	'08	'09	'10
SRRL	Golden, CO	X	X	X	X	X	X
NWTC	Boulder, CO	X	X	X	X	X	X
NPCS	Las Vegas, NV		X	X	X	X	
UNLV	Las Vegas, NV		X	X	X	X	X
HSU	Arcata, CA				X	X	
LMU	Los Angeles, CA					X	X
SSO	Monte Vista, CO					X	

B. Statistical Distributions

The probability density function is used to characterize the range of values that a random variable can take, as well as the likelihood of a sample falling in an interval. To help characterize the observed distributions of GHI changes, we will utilize two further statistical measures, in addition to the standard deviation and mean. The third standardized moment, skewness (γ), is a measure of the asymmetry of the probability distribution. A positive skew is one where more of the values lie on the left side of the mean and the right side has a longer tail, while a negative skew indicates the opposite. The fourth standardized moment, kurtosis (κ), is a measure of the peakedness of the distribution, as well as the thickness of the distribution tails. Distributions with high kurtosis values are known as leptokurtic and those with small values platykurtic. Leptokurtic distributions have more pronounced peaks, slimmer shoulders, and longer tails when compared to a normal distribution with the same variance. The difference between the kurtosis of a sample distribution and that of the normal distribution is known as the excess kurtosis. In the rest of this work, kurtosis will be treated synonymously with excess kurtosis since the normal distribution is used as a baseline distribution.

III. Results

Having established the importance of characterizing solar GHI variability and described the relevant statistical background, we now characterize the distributions for the datasets under consideration. In Section III-A, we compare the statistical distribution of solar GHI changes at varying timescales through both graphical and numerical techniques. Section III-B presents a further disaggregation of the data by examining the changes that occur during different weather patterns.

A. Distribution of Ramps by Timescale

In this analysis, we examine the changes in GHI values at each of the sites at five different timescales. The original data provides 1-minute averages, and additional datasets were created by averaging the 1-minute values over 5, 15, 30, and 60-minute intervals. As would be expected, the volatility of the data decreases with increasing timescale because the averaging serves as a low pass filter. This is illustrated in Fig. 1, where the same daily data is shown at different levels of aggregation.

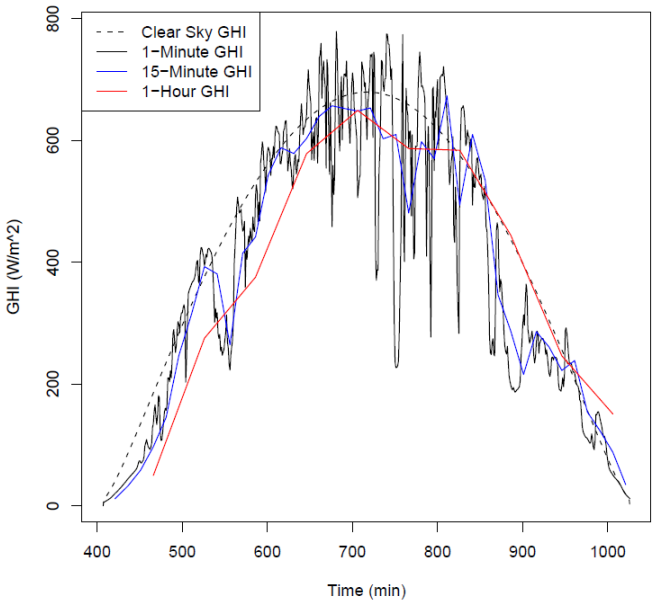

Fig. 1. Plot of the GHI ramps during the daylight hours on February 7th, 2007 at site #8. The 15-minute and 1-hour series are trailing averages over those timeframes. The clear sky time series shows the expected output with no cloud activity.

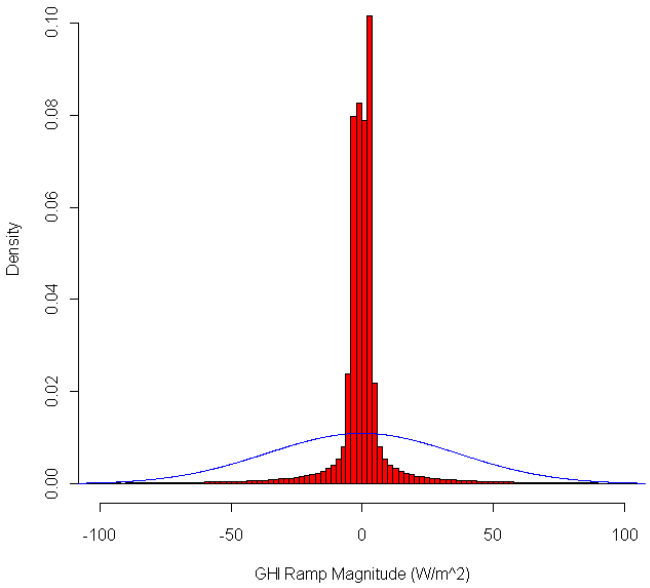

Fig. 2. Histogram of the one-minute GHI ramps over a 1-year period at site #20. γ = -0.199; κ = 70.12. The blue line represents a normal distribution with the same mean and standard deviation. The number of bins used in this example is n = 1000.

Histograms

Histograms of the data provide graphical representations of the GHI ramps that are useful for noticing patterns and making comparisons with model distributions. The number of bins used exceeded the number needed according to Scott's rule [12] in all of the examples, and a value of $n = 200$ was found to work well for most of the timescales and weather pattern combinations. Fig. 2 presents a comparison between the one minute GHI ramps observed at site #20 with a normal distribution that has the same mean and standard deviation. It is important to note that this figure is a magnified view centered on the bulk of the observations; the large standard deviation is caused by a relatively small number of observed ramp events with magnitude outside of the scale of the current figure. The histogram is very peaked, demonstrating a high kurtosis value and indicating a large number of very small magnitude ramps, along with a small but significant amount of ramps with large magnitudes. Additionally, the distribution is fairly symmetric, with only a relatively small negative skew. As may be seen in Tables II and III, the kurtosis and skewness values for this particular site are fairly typical of the 1-minute ramp distributions for all of the sites.

Fig. 3 shows a histogram of the 15-minute GHI ramps for site #19. The distribution displays a much smaller kurtosis value than the 1-minute ramp distribution, but still possesses a pronounced peak and has clearly visible heavy tails. The distribution also has a slightly positive skew, with larger magnitude instances visible on the positive side. Once again, this is a typical site for the 15-minute ramp distributions and the decreasing kurtosis values for the larger timescale confirm the decreasing variability of the datasets with the application of the averaging low pass filter. As the distributions increase in timescale, they tend to become more normal in nature with distribution mass being transferred from the peak to the shoulders.

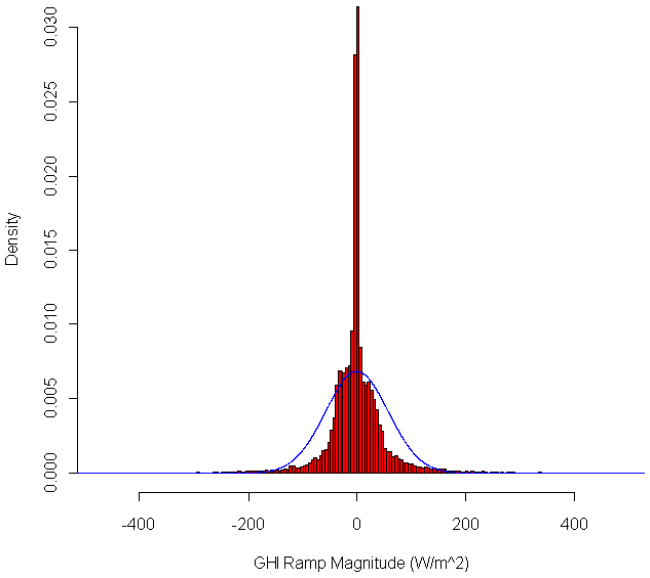

Fig. 3. Histogram of the 15-minute GHI ramps over a 1-year period at site #19. γ = 0.368; κ = 11.42. The blue line represents a normal distribution with the same mean and standard deviation. The number of bins used in this example is n = 200.

Normal Quantile –Quantile Plots

One way that two different distributions may be compared is by the examination of a quantile-quantile (Q-Q) plot. A normal Q-Q plot is one in which the observed distribution is compared to the normal distribution. While the histograms of GHI ramps strongly suggest the distributions to be non-normal, the Q-Q plots provide additional reassurance. As may be seen in fig. 4, the one-minute GHI ramps at site #5 clearly exhibit non-normal behavior. At the one minute level the high degree of kurtosis evidenced by the near horizontal points between the first and third quartiles in the Q-Q plot is typical for all of the sites. If the observed distribution were normal in nature, the Q-Q plot would display a relatively straight line running from the bottom left of the figure to the top right.

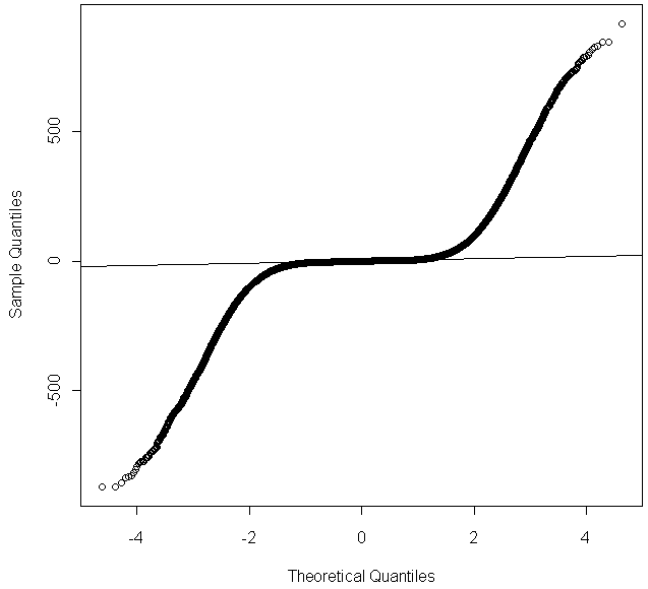

Fig. 4. Normal Q-Q plot for the 1-minute GHI ramps at site #5. γ = -0.069; κ = 47.04. The line in the graph passes through the first and third quartiles of the observed data and should run through all of the data points if the distribution is normal.

Fig. 5 shows an example Q-Q plot for the 60-minute GHI ramps from site #23. While the length of the flat section is shorter than for the one minute ramps, the plot still shows a significantly non-normal distribution, despite a kurtosis value that is seven times less than the preceding 1-minute example. These two Q-Q plots are fairly typical for the timescales under consideration and once again demonstrate the trend of increasing normality of the observed GHI ramp distributions with increasing timescale. Additional confirmation of the non-normality of the data can be provided through the use of numerical tests of distributional adequacy. The Shapiro-Wilk test [13] was run for both of the datasets displayed in Figs. 4 and 5, with the null hypothesis, that the observed GHI ramp data comes from a normal distribution, being rejected at a significance level of α = 0.000001, i.e., the 99.9999% confidence interval.

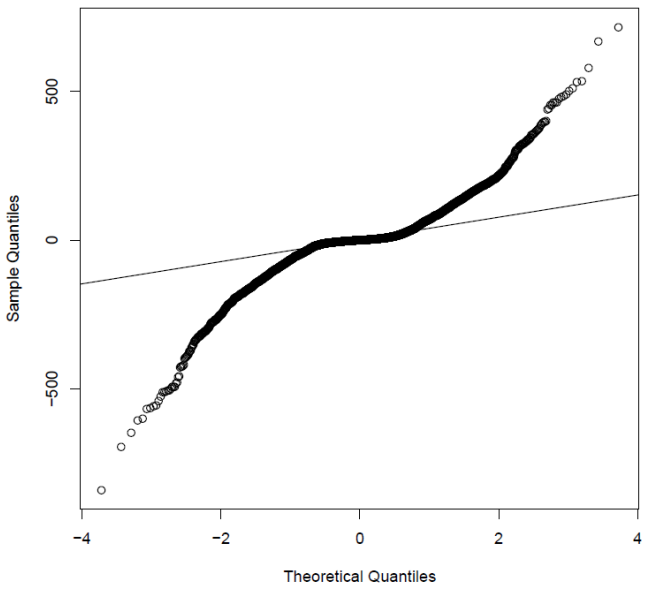

Fig. 5. Normal Q-Q plot for the 60-minute GHI ramps at site #23. γ = -0.345; κ = 7.05. The line in the graph passes through the first and third quartiles of the observed data and should run through all of the data points if the distribution is normal.

Skewness

One tool that may be used to more fully characterize the GHI ramps is calculating the skewness of the distribution. The skewness is a measure of the symmetry of the distribution and can be useful for identifying if the ramping events occur more frequently, or with greater magnitude, in the up or down direction. The skewness values for the GHI ramp distributions at each site and over the timescales considered are given in Table II. While the relatively low values that are common throughout the datasets and timescales shown indicate that the distributions are fairly symmetric, there is a slight trend toward negative skew. This indicates that while positive ramps occur slightly more frequently, the negative ramps tend to be larger in magnitude. This can partially be explained by the phenomenon of cloud focusing events, especially for the smaller timescales considered. It often occurs that during a period of clear sky just before a cloud passes over the spot of irradiance measurement there will be a brief period where the measured irradiance will be significantly greater than the estimated clear sky value. This occurs because of a greater reflection of light from the soon-to-pass-over cloud onto the spot of measurement. This temporarily raises the measured irradiance so that when the cloud does pass over, the magnitude of the decrease in measured irradiance may be greater than expected irradiance level at that time.

TABLE II
SKEWNESS VALUES FOR THE DATASETS AT THE CONSIDERED TIMESCALES

Site	*1-Min*	*5-Min*	*15-Min*	*30-Min*	*60-Min*
1	*-0.064*	*-0.228*	*-0.323*	*-0.331*	*-0.234*
2	*-0.907*	*-0.150*	*-0.453*	*-0.384*	*-0.331*
3	*-0.328*	*-0.013*	*-0.109*	*-0.251*	*-0.175*
4	*-0.166*	*-0.022*	*0.143*	*-0.195*	*-0.333*
5	*-0.069*	*-0.063*	*-0.262*	*-0.586*	*-0.584*
6	*-1.517*	*-0.105*	*-0.264*	*-0.188*	*-0.190*
7	*0.039*	*0.053*	*-0.071*	*0.071*	*-0.198*
8	*0.068*	*-0.188*	*-0.072*	*0.097*	*-0.057*
9	*-0.158*	*-0.312*	*-0.417*	*-0.712*	*-0.635*
10	*-0.394*	*-0.284*	*-0.408*	*-0.513*	*-0.382*
11	*-0.098*	*-0.137*	*-0.472*	*-0.523*	*-0.193*
12	*0.164*	*0.305*	*0.378*	*0.578*	*0.451*
13	*0.001*	*-0.1117*	*-0.474*	*-0.411*	*-0.379*
14	*-0.065*	*-0.261*	*-0.444*	*-0.408*	*-0.262*
15	*-1.373*	*-0.299*	*-0.192*	*-0.351*	*-0.643*
16	*-0.118*	*-0.145*	*-0.280*	*-0.304*	*-0.316*
17	*0.050*	*-0.264*	*-0.462*	*-0.624*	*-0.725*
18	*-0.161*	*0.156*	*0.074*	*0.330*	*0.308*
19	*0.034*	*-0.035*	*0.368*	*0.447*	*0.427*
20	*-0.167*	*-0.180*	*-0.617*	*-0.746*	*-0.859*
21	*-0.149*	*-0.118*	*-0.532*	*-0.868*	*-0.948*
22	*-2.248*	*-0.073*	*-0.221*	*-0.131*	*-0.172*
23	*-0.115*	*-0.145*	*-0.369*	*-0.442*	*-0.345*
24	*0.231*	*0.399*	*0.868*	*0.311*	*0.180*
25	*-0.046*	*-0.120*	*0.054*	*-0.145*	*0.003*
26	*-0.004*	*-0.124*	*-0.068*	*-0.270*	*-0.365*

Kurtosis

Another way of characterizing the distribution of GHI ramps is an examination of their fourth moment, i.e., kurtosis. As was seen in Figs. 2 and 3, the observed ramp distributions are very strongly peaked, indicating a large

number of very small changes, with the variance mostly due to a smaller number of large changes. Measuring the kurtosis of the distribution provides a means to compare the relative frequency of large and small ramps between different sites and timescales. As may be seen in Table II, every one of the GHI ramps distributions studied has a kurtosis value that exceeds the normal distribution, often significantly so. It is important to recall here our previous definition of kurtosis as excess kurtosis, so that the kurtosis of a normally distributed dataset would give a kurtosis value of zero. In addition, the decreasing volatility with increased timescale, due to the effects of averaging the data over those timescales, is also clearly visible in the decreasing trend of kurtosis values at longer timescales. This provides numerical evidence for the phenomenon demonstrated in Fig. 1, and is a result of the central limit theorem. This is most visible in the strong decrease in kurtosis values between the 1-minute and 5-minute datasets, as this is the largest proportional aggregation of the data considered among the timescales shown.

TABLE III
KURTOSIS VALUES FOR THE DATASETS AT THE CONSIDERED TIMESCALES

Site	*1-Min*	*5-Min*	*15-Min*	*30-Min*	*60-Min*
1	*50.11*	*22.53*	*13.54*	*11.02*	*7.46*
2	*146.38*	*22.86*	*13.46*	*9.96*	*6.18*
3	*101.99*	*42.56*	*24.59*	*13.15*	*5.30*
4	*108.44*	*40.38*	*24.69*	*14.64*	*6.85*
5	*47.04*	*21.49*	*12.89*	*9.41*	*7.24*
6	*246.96*	*22.27*	*13.45*	*9.46*	*6.73*
7	*105.14*	*40.16*	*26.79*	*22.58*	*18.48*
8	*87.49*	*39.77*	*23.19*	*19.41*	*17.02*
9	*51.18*	*23.87*	*15.75*	*15.49*	*8.96*
10	*75.88*	*20.74*	*13.66*	*10.12*	*7.80*
11	*89.74*	*43.33*	*26.89*	*14.36*	*9.32*
12	*51.87*	*22.82*	*11.87*	*7.21*	*2.48*
13	*78.95*	*39.81*	*24.35*	*21.64*	*20.30*
14	*59.83*	*26.74*	*16.12*	*9.75*	*3.97*
15	*217.24*	*22.53*	*12.82*	*9.93*	*6.50*
16	*48.77*	*19.52*	*12.92*	*9.47*	*6.93*
17	*69.67*	*30.45*	*19.88*	*14.90*	*12.11*
18	*94.74*	*40.28*	*22.28*	*13.10*	*6.77*
19	*49.33*	*24.82*	*11.42*	*5.85*	*2.53*
20	*70.64*	*30.602*	*20.41*	*16.97*	*13.52*
21	*50.15*	*22.50*	*16.52*	*14.90*	*11.72*
22	*336.15*	*22.68*	*13.12*	*10.11*	*6.94*
23	*43.20*	*20.21*	*12.50*	*8.99*	*7.05*
24	*60.27*	*42.91*	*21.87*	*4.20*	*0.22*
25	*79.89*	*34.88*	*21.87*	*11.75*	*5.53*
26	*45.32*	*21.76*	*13.36*	*9.98*	*6.97*

Distribution Fitting

Having established that the normal distribution provides an inaccurate representation of the ramps found in single site solar measured GHI, we provide an alternative parametric distribution that can be used to model the observed distribution. The hyperbolic distribution provides a more accurate representation of the distinct peaks and heavy tails found in the observed distributions. The tails of the distribution decrease exponentially, which is more slowly than for the normal distribution, and hence is better able to capture more of the observed tails of the distribution. Distribution parameters were fit to the data using a maximum likelihood method implemented in the *hyperbFit* function of the *HyperbolicDist* package [14] in the *R* statistical computing environment [15]. A typical example from the datasets of how a fit hyperbolic distribution can more accurately represent the observed GHI ramps than a normal distribution with the same mean and variance is shown in Fig. 6. The hyperbolic distribution fit to the 1-minute GHI ramps for site #12 is more peaked and has heavier tails than normal distribution shown. Visual inspection shows that while the fit of the model distribution to the observed distribution is not perfect, it provides a more accurate representation of the observed distribution's pronounced peak and slim shoulders than a normal distribution with the same mean and standard deviation.

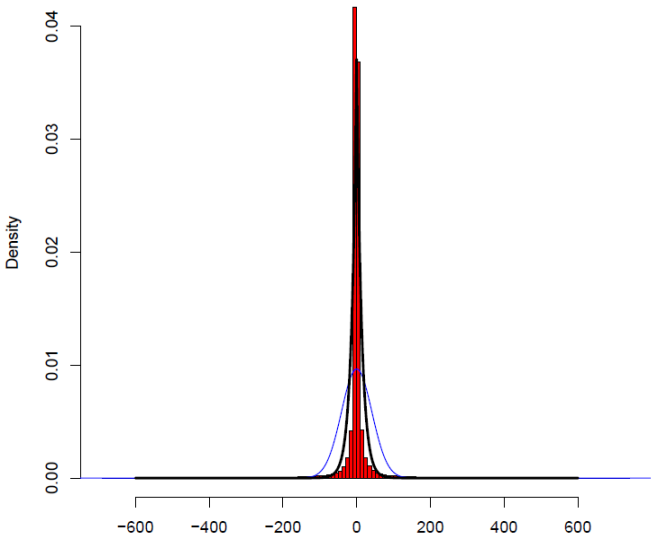

Fig. 6. Histogram of the one minute GHI ramps for site #12. The blue line represents a normal distribution with the same mean and standard deviation. The black line represents a hyperbolic distribution fit to the data with: $\pi = 0.0050$, $\zeta = 0.0001$, $\delta = 0.0015$, $\mu = -0.1305$.

B. Distribution of Ramps by Weather Pattern

In the absence of other sources of time-correlated weather data, we utilize a simple technique for classifying different types of weather patterns. For each measurement site, clear sky GHI values were computed for each minute of the year based solely on the position of the sun for each day and a clear sky assumption using the Bird clear sky model. We refer to these values as the clear sky irradiance values. Current weather patterns were then roughly classified by normalizing the measured GHI value by the clear sky GHI value for the previous three time steps. Despite the higher variability at the smaller timescales, this simple classification method was found to be more effective for the smaller timescales due to the larger number of qualifying instances.

Three broad classifications were used: clear sky, intermittent cloud activity, and overcast. To demonstrate the differences in GHI ramps between these three weather pattern classifications, we examine the distribution of GHI ramps from each weather pattern for the same site and at the same timescale. The 5-minute timescale at site #26 was chosen because it serves as a good example of the differences between weather pattern ramp distributions. When examining the histograms it is important to notice the differences in the y-axis scale, while the x-axis scale

remains constant due to the normalization of ramp magnitudes.

Clear Sky Conditions

When there is no cloud activity, the measured irradiance data will have considerably reduced variability. During these times, the measured irradiance data will match the clear sky profiles reasonably well, with only relatively minor deviations from the expected irradiance levels. The criteria for classifying a period as clear sky is that the normalized GHI value is between 0.95 and 1.05; i.e., between 95% and 105% of the expected clear sky value for each of the previous three time steps. The upper bound is necessary due to cloud focusing events that can temporarily cause the measured GHI to far exceed the expected clear sky value, and are usually followed by a sharp drop in GHI, indicating intermittent cloud activity conditions are a better classification. Fig 7 shows the histogram of averaged 5-minute GHI ramps classified in the clear sky weather pattern. Immediately noticeable is the small degree of variability in the distribution, as indicated by the very large kurtosis value and small standard deviation of the associated normal distribution. Since most changes in measured GHI are due to the effects of clouds, once a time period has been identified as having a clear sky, most non-diurnal changes in measured GHI are relatively small. Another interesting aspect is the relatively large skewness positive skewness value. Since we are examining only the time periods immediately following clear sky conditions, this indicates a large number of occurrences of an increase in the measured GHI level to above that predicted by the clear sky model. Since we only examine a single data point past the clear sky classification, these data points capture the effects of cloud focusing events that temporarily increase the measured GHI before a large drop in GHI occurs due to the passing of a cloud.

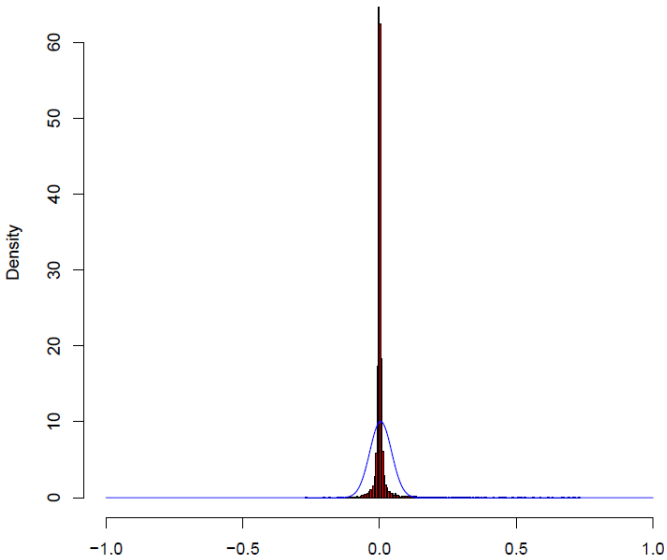

Fig. 7. Histogram of the 5-minute GHI ramps over a 1-year period at site #26 for periods classified in the clear sky weather pattern. $\gamma = 9.17$; $\kappa = 119.89$. The blue line represents a normal distribution with the same mean and standard deviation. The number of bins used in this example is n = 200.

Intermittent Cloud Activity Conditions

Irradiance measurements can vary quickly when, during a period of otherwise clear sky, a cloud momentarily passes overhead. The magnitude and speed of the change in irradiance are dependent on the time of day and type of clouds present, and thus can vary widely. Therefore, periods of intermittent cloud activity are characterized by larger than normal variability. We use a normalized GHI value in the range of 0.4 to 0.9 during the previous three time periods to classify intermittent cloud activity. The increased variability seen during times of intermittent cloud activity is immediately apparent in Fig. 8. The kurtosis value for this distribution is significantly less than for the clear sky weather pattern distribution and the standard deviation of the associated normal distribution is much greater. The distribution is also slightly negatively skewed, indicating that large decreases are slightly more likely than large increases.

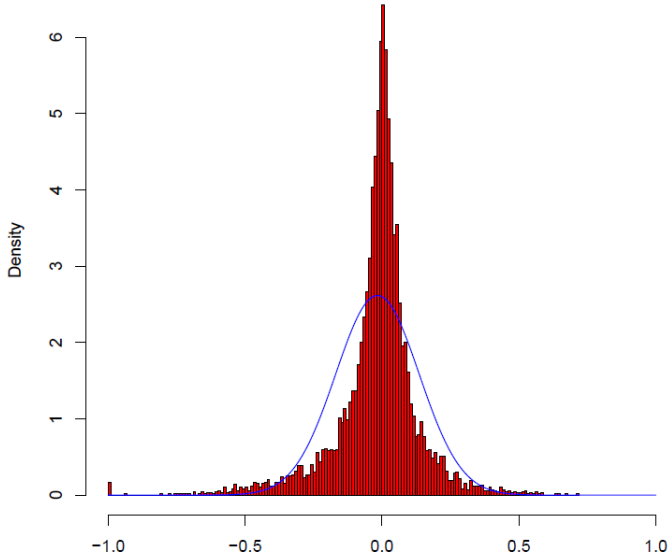

Fig. 8. Histogram of the 5-minute GHI ramps over a 1-year period at site #26 for periods classified in the intermittent cloud activity weather pattern. $\gamma = -1.05$; $\kappa = 5.99$. The blue line represents a normal distribution with the same mean and standard deviation. The number of bins used in this example is n = 200.

Overcast Conditions

During periods that can be described as overcast, the measured irradiance level is typically much lower than the expected clear sky value. While the measured GHI values are often lower than during periods of intermittent cloud activity, the measured variability in the overcast case is often less because the magnitude of changes is smaller. That is, when the weather is generally overcast, there are less large magnitude changes because the range of measured GHI values is effectively limited to well below the clear sky value. Classification as a period with overcast conditions was made based on a normalized GHI value below 0.4. As seen in Fig. 9, the time periods classified as overcast have less variability than those in the intermittent cloud activity weather pattern, as evidenced by the larger kurtosis value. The relatively large negative skew indicates that larger magnitude ramps occur more often in the downward direction than in the upward direction. This indicates the persistence of overcast conditions once they have been experienced, as it is very rare to go from an overcast measurement to a near clear sky measurement, but a further reduction in GHI from the current level is seen often.

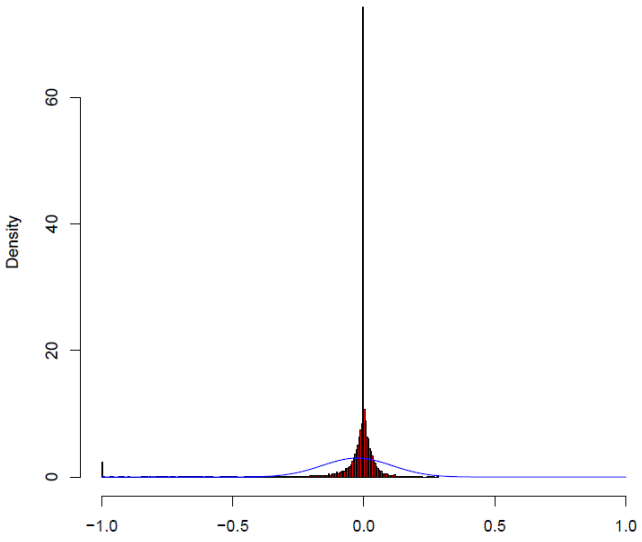

Fig.9. Histogram of the 5-minute GHI ramps over a 1-year period at site #26 for periods classified in the overcast weather pattern. γ = -5.74; κ = 36.64. The blue line represents a normal distribution with the same mean and standard deviation. The number of bins used in this example is n = 200.

Implications of Ramp Distributions by Weather Pattern

The observed differences in variability between the classified weather pattern types has implications for both solar power output forecasting, as well as the synthesis of solar data for integration studies. Solar PV installations are often placed in locations that are judged to have the best resource. In the case of solar power, this means locations that consistently experience extended periods of clear sky. This is important when synthesizing a dataset of solar irradiance at one of these locations. Using a single distribution to create variability in the dataset would significantly overestimate the variability during a large number of days during the year, if the distribution is based on a yearly metric, such as standard deviation of ramps. As evidenced by the clear sky weather pattern histogram in Fig. 7, the variability during periods of clear sky is significantly less than during the year as a whole. A similar problem could occur when producing confidence intervals on a solar irradiance forecast. If a single model distribution is used to create the confidence intervals around a point forecast for every time period, the uncertainty around the forecast would be significantly overstated during times of clear sky or overcast weather patterns. On the other hand, the uncertainty could be understated during times of intermittent cloud activity. The large differences in variability between easily identifiable and simply classified weather patterns suggest that more refined disaggregation techniques should be applied to both solar data uncertainty forecasting, as well as data synthesis algorithms.

IV. Conclusion

In this paper, we have examined the shapes of solar irradiance ramping distributions at multiple timescales and during different weather conditions through a statistical analysis. The characterization of ramping distributions can be important for creating solar power forecasts, as well as synthesizing solar irradiance data for integration studies. The distribution of GHI ramps at timescales ranging from 1-minute to 1-hour were shown to be significantly non-normal for 26 datasets, consisting of 7 different measurement sites and 6 different years. The distributions were found to be increasingly leptokurtic with decreasing timescale and a hyperbolic distribution was suggested as an alternative model distribution. Portions of the GHI datasets were also classified into three categories, representing three commonly observed weather patterns. The distribution of GHI ramps was found to differ significantly between classified weather patterns. This suggests that individually developed model distributions should be used to characterize the variability of solar irradiance during different weather regimes.

Employees of the Alliance for Sustainable Energy, LLC, under Contract No, DE-AC36-0BG02830B with the U.S. Dept. of Energy have authored this work. The United States Government retains and the publisher, by accepting the article for publication, acknowledges that the United States Government retains a non-exclusive, paid-up, irrevocable, worldwide license to publish or reproduce the published from of this work, or allow others to do so, for United States Government purposes.

V. References

[1] A. Mills, M. Ahlstrom, M. Brower, A. Ellis, R. George, T. Hoff, B. Kroposki, C. Lenox, N. Miller, M. Milligan, J. Stein, and Y.-H. Wan. (2011) Dark Shadows: Understanding Variability and Uncertainty of Photovoltaics for Integration with the Electric Power Systems. *IEEE Power & Energy Magazine*. 33 - 41.

[2] J. Marcos, L. Marroyo, E. Lorenzo, D. Alvira, and E. Izco, "Power output fluctuations in large scale PV plants: one year observations with one second resolution and a derived analytic model," *Progress in Photovoltaics: Research and Applications,* vol. 19, pp. 218 - 227, 2011.

[3] J. Marcos, L. Marroyo, E. Lorenzo, D. Alvira, and E. Izco, "From irradiance to output power fluctuations: the pv plant as a low pass filter," *Progress in Photovoltaics: Research and Applications,* vol. 19, pp. 505 - 510, 2011.

[4] E. Wiemken, H. G. Beyer, W. Heydenreich, and K. Kiefer, "Power Characteristics of PV Ensembles: Experiences from the Combined Power Production of 100 Grid Connected PV Systems Distributed over the Area of Germany," *Solar Energy,* vol. 70, pp. 513 - 518, 2001.

[5] A. Curtright and A. J., "The Character of Power Output from Utility-Scale Photovoltaic Systems," *Progress in Photovoltaics: Research and Applications,* vol. 16, pp. 241 - 247, 2008.

[6] M. Lave and J. Kleissl, "Solar variability of four sites across the state of Colorado," *Renewable Energy,* vol. 35, pp. 2867 - 2873, 2010.

[7] M. Varo, G. Pedros, P. Martinez-Jimenez, and M. Aguilera, "Global solar irradiance in Cordoba: Clearness index distributions conditioned to the optical air mass," *Renewable Energy,* vol. 31, pp. 1321 - 1332, 2006.

[8] A. Woyte, R. Belmans, and J. Nijs, "Fluctuations in instantaneous clearness index: Analysis and statistics," *Solar Energy,* vol. 81, pp. 195 - 206, 2007.

[9] J. Ma, Y. Makarov, C. Loutan, and Z. Xie, "Impact of Wind and Solar Generation on the California ISO's Intra-hour Balancing Needs," in *IEEE Power & Energy Society General Meeting*, Detroit, MI, 2011.

[10] NREL. (2011). *Measurement and Instrumentation Data Center*. Available: http://www.nrel.gov/midc/

[11] R. Bird and R. Hulstrom, "A Simplified Clear Sky Model for Direct and Diffuse Insolation on Horizontal Surfaces," Solar Energy Research Institute, Golden, CO1981.

[12] D. Scott, "On optimal and data-based histograms," *Biometrika,* vol. 66, pp. 605-610, 1979.

[13] S. Shapiro and M. Wilk, "An analysis of variance test for normality (complete samples)," *Biometrika,* vol. 52, 1965.

[14] D. Scott, "HyperbolicDist: The hyperbolic distribution," ed, 2009.

[15] "R: A Language and Environment for Statistical Computing," ed. Vienna, Austria: R Foundation for Statistical Computing, 2010.

Bri-Mathias Hodge received the B.S. degree in chemical engineering from Carnegie Mellon University, Pittsburgh, PA. He received a M.S. from Åbo Akademi, Turku, Finland, and completed the Ph.D. in chemical engineering at Purdue University, West Lafayette, IN. He is currently a researcher engineer in the Transmission and Grid Integration Group at NREL. His research interests include energy systems modeling, simulation, optimization, and analysis.

Marissa Hummon received the B.A. degree in physics from Colorado College, Colorado Springs, CO and the Ph.D. degree from the Harvard University, Cambridge, MA in applied physics. She joined the NREL Strategic Energy Analysis Center to work on energy forecasting models. Her work focuses on spatial statistical analysis of multi-point time-series data including irradiance, PV power plant production, and advanced grid measurements (smart grid components). She applies analyses to models and simulations, such as sub-hourly photovoltaic power generation and smart grid measurement and control operation in production cost modeling. Her fields of interest include large-scale grid modeling, sub-hourly variable renewable modeling, and applied mathematics.

Kirsten Orwig completed her M.S. in Atmospheric Science and Ph.D. in the Wind Science and Engineering at Texas Tech University, researching the turbulence characteristics of high wind events through the use of traditional and nontraditional statistical methods. She joined NREL in 2009 to provide statistical and meteorological support for the Transmission & Grid Integration Group. She is researching and developing methods to quantify wind and solar energy variability, evaluating the impacts of variability on utilities, and developing techniques to model the impacts. She is also coordinating all of the solar transmission grid integration activities at NREL.